Multipactor-triggering powers' modelling of a WEST ICRH antenna during RF conditioning

Eva Al Hajj Sleiman, Julien Hillairet, Mohamed Belhaj

Multipactor-Triggering Powers' Modelling of a WEST ICRH Antenna during RF Conditioning

Eva Al Hajj Sleiman[1, 2], Julien Hillairet[1], and Mohamed Belhaj[2]

[1]CEA, IRFM, 13108 Saint Paul Les Durance, France
[2]ONERA, DPHY, Université de Toulouse, 31055 Toulouse, France

***Abstract*— During RF conditioning of the ion cyclotron resonance heating (ICRH) system on WEST, under vacuum, pressure rises are measured inside the antennas. A proposed hypothesis for the cause of this phenomenon is multipactor, an electron multiplication process taking place in RF devices under vacuum. Modelling multipactor conditions in a resonant antenna, *i.e.*, under high standing wave ratio, requires particular precautions. This paper proposes a methodology to determine the multipactor conditions in such a context. Using the proposed approach, the operational conditions, expressed as the generator's RF powers, of the appearance of multipactor inside a WEST ICRH antenna during its RF conditioning under vacuum, are deduced. Calculations are performed for two different surface states: when the surface is baked but *non-conditioned*, and when it is baked and *fully conditioned*. For the *non-conditioned* surface state, it is shown that when only one side of the under-conditioning ICRH antenna is powered, the off-mode side is prone to multipactor when its capacitors are tuned. Detuning the capacitors on the off-mode side suppresses almost the multipactor on the non-powered side for the frequency range of interest. Moreover, it is shown that the *fully conditioned* antenna surface state can suppress the appearance of multipactor in some regions of the antenna.**

Keywords: Ion Cyclotron Resonance Heating (ICRH), multipactor, conditioning, Total Electron Emission Yield (TEEY)

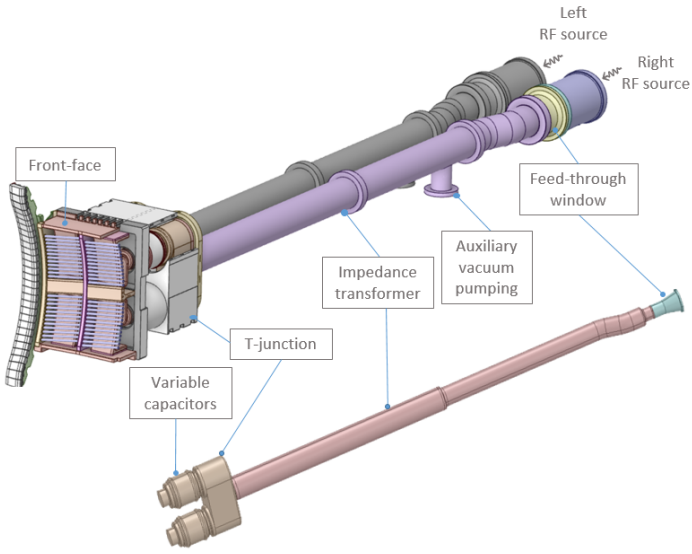

Fig. 1. Top – An illustration of the different components of one ICRH antenna used on the tokamak WEST. Each side has its own high-power generator. Bottom – The inner conductor representation of the feed-through window, impedance transformer, and T-junction.

I. Introduction

Ion cyclotron resonance heating (ICRH) is one of the possible plasma heating systems for fusion reactors. It is commonly used in experimental magnetic confined nuclear fusion experiments. In the WEST tokamak located at CEA/Cadarache, France, the ICRH system consists of three identical four straps-antennas. These antennas are operated in the frequency range $[46 - 65]$ MHz [1], [2].

Each WEST ICRH antenna is composed of two sides: *left* and *right*. Each side is constituted of two variable capacitors, a passive three-ports of T-junction type called "bridge", a two-step impedance transformer, used to match the impedance of the main transmission line ($30\,\Omega$) to the low T-junction impedance, and an RF feed-through made with an alumina ceramic. The RF feed-through ensures the tightness between the vacuum-pumped part on the tokamak side and the Nitrogen-pressurized parts of the coaxial transmission lines connected to the RF generators. An illustration of the different components of one ICRH antenna is given in Fig.1. Each side has its own RF power generator so that either one or both sides of the antenna can be powered, generally in dipole phasing ($180°$ phase shift between sides). Each antenna side's high-power generator can provide up to $1.5\,\mathrm{MW}$, hence leading to up to $3\,\mathrm{MW}$ per antenna.

Before each WEST experimental campaign, the tokamak and its heating systems are baked up to $200\,°\mathrm{C}$. During plasma operations, the machine and the antennas are water-cooled at $70\,°\mathrm{C}$. Before using the ICRH system on plasma, a preliminary RF conditioning phase is performed during the tokamak commissioning. During RF conditioning under vacuum, each side of the antenna is powered separately on short pulses until reaching the voltage's limit for not exceeding the maximum current of the antenna's capacitors ($< 27\,\mathrm{kV}$). During this step, pressure rises are measured inside the antenna, by vacuum gauges connected to the rear of each impedance transformer, in association with an auxiliary pumping system (Fig.1). In addition, visible light, RF sub-harmonics, and reflected power are observed during this conditioning phase [2]. One possible cause explaining these observations is the multipactor phenomenon, a resonant RF vacuum discharge [3]. This paper proposes a generic methodology to determine how and where multipactor discharges can be triggered, during realistic operational scenarios, in complex geometries such as a WEST ICRH

antenna. As an example, this generic methodology is applied to the case of a single ICRH antenna operated during the RF vacuum conditioning phase and without a toroidal magnetic field. In such a case, the standing waves and the cross-talk between the sides of a single antenna are not negligible and must be taken into account self-consistently.

The paper is organized as follows: Section II recalls the definition of the multipactor phenomenon and lists the required conditions for its ignition and sustainability. Section III details the methodology used to solve the problem. Section IV presents the results obtained and discusses the main findings before concluding in Section V.

II. Multipactor Definition and Conditions

Multipactor is an electron avalanche caused by secondary electron emission from the surfaces of an under-vacuum radio-frequency (RF) device. For all-metallic devices where the electric field is normal to the surfaces, the multipactor occurs when some primary electrons, which are accelerated by the RF field, impact a surface and cause a release of additional secondary electrons. Released electrons are also accelerated by the electric field and release additional secondary electrons after impacting a surface of the device. This mechanism can lead to an electron avalanche [3], which can cause electrical discharge and damage to the equipment. In a metal coaxial geometry, such discharges can occur on a single conductor surface or between the inner and the outer conductor surfaces [4].

Although this phenomenon could be beneficial for some signal amplification applications [5], this is not the case for many applications: such as RF satellite payloads, particle accelerators [6], accelerating cavities [7], vacuum tubes or experimental fusion reactors' heating systems [8]–[10].

In the RF heating systems of nuclear fusion devices, multipactor electron cloud can induce reflected power (detuning), create outgassing, and increase components' temperature [11]. These effects can ultimately lead to RF breakdowns with the following consequences: metallization of the vacuum feed-through ceramics (called RF windows) by arc-induced sputtering [12], or corona discharges [13], [14].

In all-metallic devices, such as the ones studied in this paper, for this resonant secondary electron emission mechanism [15] to occur, two conditions must be simultaneously fulfilled [3]. *i)* The impact energy of electrons colliding with a surface of the structure must be sufficient to emit more electrons from the surface than the impinging electrons. In electron emission terminology, this condition means that the electrons' impact energy should exceed the first cross-over energy of the material while remaining lower than the second cross-over energy so that the total electron emission yield (TEEY) of the electrodes' surface is greater than one [16], [17]. *ii)* The synchronization (resonance) between the electrons' motion and the phase change of the RF electric field. The first condition depends on the material surface's properties and is known to affect largely the multipactor's occurrence [18]. For this reason, it is essential to properly characterize the secondary emission properties in conditions relevant to the RF device operation. The TEEY characteristics of the WEST ICRH antenna are detailed in the next section, followed by a description of the methodology used for the multipactor thresholds calculation.

A. TEEY characteristics within WEST relevant operational conditions

Before operating the RF heating system on vacuum or plasma, the ICRH antennas are subject to in-situ conditioning treatments: baking (during the general tokamak baking) and RF conditioning. RF conditioning is an antenna-surface conditioning technique based on short RF power pulses (ms), used to clean and remove impurities deposited on the surfaces [19]. In some conditions that we would like to identify, these RF power pulses trigger multipactor inside the different components of the antenna. Multipactor discharges – among other possible phenomena – are known to be responsible for the elimination of hydrocarbon elements, and adsorbed hydroxides from the surfaces of the antennas' components [19]. As a result of baking and RF conditioning, the emission properties of the antenna's surfaces are modified. As in [19], the RF conditioning is mimicked by an in-situ electron bombardment.

Therefore, accurate knowledge of the materials' TEEY characteristics is essential for conducting proper multipactor analysis [18]. The TEEY of the silver-coated surfaces of the WEST ICRH antennas has been measured for relevant operational baking temperature, baking duration, and surface temperature ($70\,^{\circ}\mathrm{C}$) in [19]. The results are briefly summarized here. This paper analyzed two extreme situations (Fig. 2): *i)* the TEEY measurements before any conditioning treatment, represented in red, for a silver-coated sample baked for three days at $200\,^{\circ}\mathrm{C}$, and maintained at $70\,^{\circ}\mathrm{C}$. This situation characterizes the surface characteristics of the antennas at the beginning of the RF conditioning phase and can be considered the worst situation. We refer to these TEEY measurements as *"non-conditioned"*. The TEEY measurements, for the same baked sample, after the saturation of the TEEY properties (where the first crossover energy and maximum TEEY can no more be reduced with additional conditioning on the sample's surface) represented in black [19], which we refer to as *"fully conditioned"*. These latter measurements characterize the antennas' surface properties mimicking the end of the RF conditioning phase.

The TEEY of the conditioned surfaces is reduced, reducing hence the multipactor occurrence. The latter observation is corroborated in practice, as RF operators see a progressive increase in the voltage standoff of the antennas (up to the nominal regime). The choice of these two extreme TEEY is motivated by the goal of determining how RF conditioning affects the antennas' vulnerability to multipactor at the beginning and the end of the RF conditioning phase.

III. Methodology

During its RF vacuum conditioning phase, operators of the ICRH antennas control, for a given frequency, the RF power of the generators feeding one or both sides of the antenna and the four internal variable capacitors. Hence, our goal is to determine the generators' forward powers and capacitor

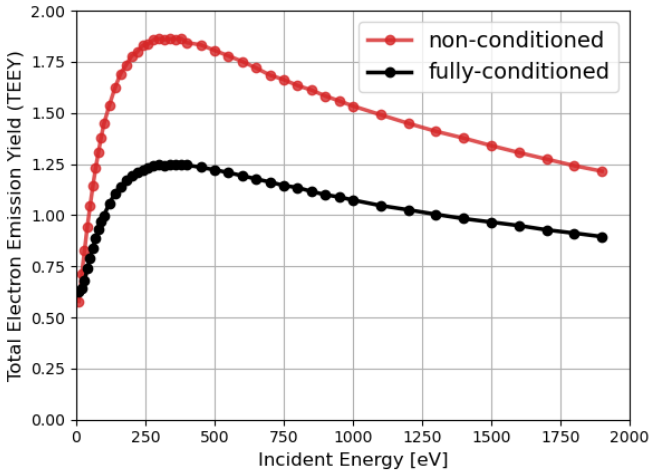

Fig. 2. TEEY measurements for a baked WEST ICRH representative silver-coated sample, maintained at 70 °C. In red, the TEEY data are measured before any conditioning treatment; and in black, the TEEY data are measured after a full conditioning treatment of the surface (with a cumulative electron dose of 2338 $\mu C\,mm^{-2}$) [19].

states that can trigger multipactor inside the different sides and components of the antenna and deduce the best strategies to reduce or avoid multipactor.

During this RF conditioning phase, there is no plasma in the vacuum vessel, and we will assume that no toroidal magnetic DC field is present. As the antennas face vacuum loading they have a very low coupling under these conditions and only a very small fraction of the generators' power is coupled into the vacuum vessel. The forward power of the generators during this phase is, in practice, limited to the range $[5-20]$ kW per antenna side, and applied during 20 ms maximum, to avoid exceeding the voltage and current limits of the variable capacitors. During the antenna conditioning phase, one antenna side is energized at a time while the other generator remains off. Once the nominal voltage across the capacitor (27 kV) is reached, both sides are energized in dipole configuration (180° phase difference between sides). Once achieving 27 kV on both sides of the antenna, the duration of the RF pulse is progressively increased, up to 5 s. As cross-talk between the two sides of one ICRH antenna can also trigger multipactor into the non-energized side, meaning we should determine the conditions triggering multipactor and the locations where multipactor is initiated on both powered and non-powered sides of the antenna. Additionally, all these results also depend on the secondary emission properties of the antenna surfaces, which itself evolves during conditioning [19].

As mentioned previously, the capacitors are variable, and there are two capacitors per antenna side (*i.e.*, four capacitors per ICRH antenna). Therefore, their capacitance can be tuned to match an antenna side at the frequency of interest. When the capacitors are tuned to match the antenna at a particular frequency, they are called *tuned capacitors*. When the capacitance of each capacitor is set to the value 120 pF (highest

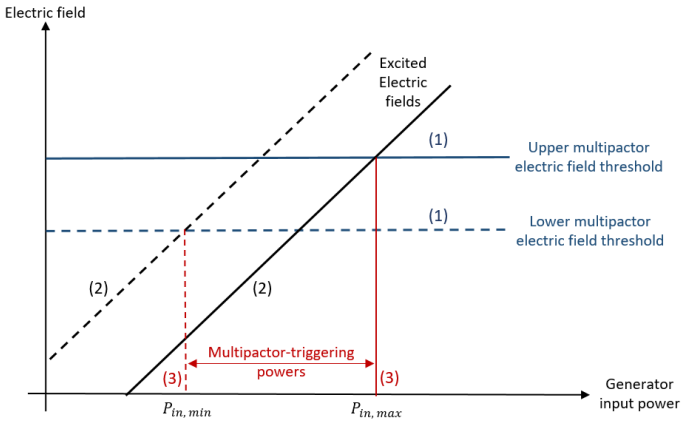

Fig. 3. Illustration of the main three steps used to solve the problem for a given frequency. The blue lines correspond to the electric field multipactor thresholds, the black lines correspond to the excited electric fields, and the red lines correspond to the resultant generators' forward powers triggering multipactor inside the geometry.

capacitance value), this configuration is called *detuned capacitors*, as the antenna side is no more resonant.

Given the fact that we have variable capacitors and two generators per antenna, three operational cases are studied:

Case 1: The generators of both sides of the antenna are on, and the capacitors of both sides are *tuned*. The antenna is operated in dipole, that is with a 180° phase difference between both sides.

Case 2: The generator of one side of the antenna (*right* or *left*) is on, the generator of the other side is off, and capacitors of both sides are *tuned*.

Case 3: The generator of one side of the antenna is on, the generator of the other side is off, and the capacitors of the powered generator are *tuned*, while the capacitors of the off-mode side are *detuned*.

To achieve our goals, the problem is divided into three main parts, illustrated schematically in Fig. 3 for a given frequency:

1) Determining the electric fields responsible for triggering multipactor inside the different components of the antenna (blue lines in Fig. 3). In this work, we deduce the multipactor electric field thresholds from multipactor power thresholds determined with Spark-3D[1] software. As our software's version only supports metallic boundary conditions and single TEEY, our study excludes the ceramic vacuum feed-through and focuses on the main components of the WEST ICRH antennas: the bridge and the impedance transformer. These thresholds are called the *multipactor electric fields thresholds* and are determined while considering the measured WEST material secondary emission properties.
2) Solving for the electric field in antenna sections, using a full-wave and a circuit solver (ANSYS Electronics). This takes into account self-consistently: the generator powers, the capacitor states, and the coupling between both sides. Thus, this step leads to the determination of the *excited*

[1] version 1.6.3

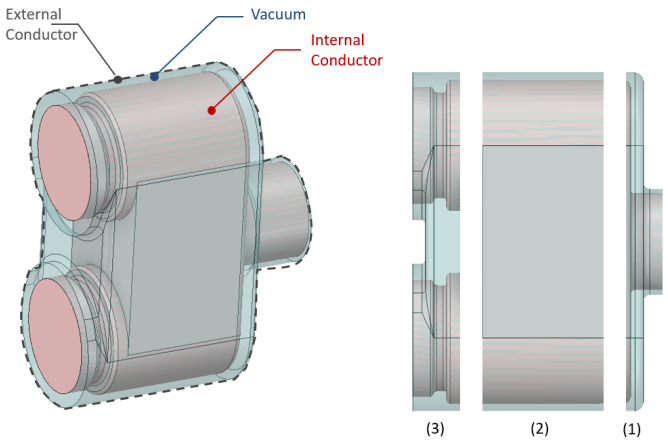

Fig. 4. Left – The design of the T-junction, where in red the inner conductor is represented, in blue the vacuum volume, and in dashed black the outer conductor Right – The cut view representation of each of the bridge multipactor regions. The bridge is divided into three different multipactor regions: (1) – *Region A*, (2) – *Region B*, and (3) – *Region C*.

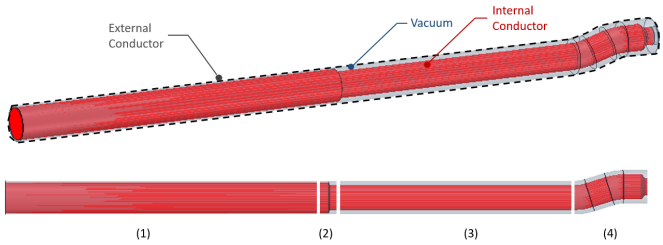

Fig. 5. Top – The design of the impedance transformer, where in red the inner conductor is represented, in blue the vacuum volume, and in dashed black the outer conductor. Bottom – The cut view representation of each of the impedance transformer multipactor regions. The impedance transformer is divided into four different multipactor regions: (1) – *Section 1*, (2) – *Transition 1*, (3) – *Section 2*, and (4) – *Transition 2*.

electric fields in all components of the antenna (black lines in Fig. 3).

3) Comparing the *multipactor electric fields thresholds* to the *excited electric fields*. It leads to the determination of the forward generators' powers (lower and upper thresholds) triggering multipactor inside the different components of the antenna (red points in Fig. 3).

In the following subsections, we elaborate these steps.

A. Multipactor Electric Fields Thresholds' Determination

To accurately determine the multipactor thresholds in the bridge and impedance transformer components, which are of complex 3D geometries, we have split each of these components into separate multipactor analysis regions. The multipactor regions are chosen such that the electromagnetic fields and/or the geometry are as much as possible homogeneous. The geometry of the bridge (represented in Fig. 4) is divided into three regions: *Region A* being close to a parallel-plates-like geometry, *Region B* a coaxial geometry of elliptical cross-section and *Region C* being the two regions connected to the capacitors, joined by a parallel-plates-like geometry. The geometry of the impedance transformer (represented in Fig. 5) is split into four regions: two circular coaxial transmission lines regions of characteristic impedance $5.5\,\Omega$ (*Section 1*) and $17.4\,\Omega$ (*Section 2*), and two complex tapered transitions geometries called *Transition 1* and *Transition 2*.

As the WEST ICRH antennas are resonant, they are subject to standing waves (SW). In standing wave conditions, it is more relevant to define the multipactor thresholds in terms of the electric field rather than power [20]–[22]. For each of the defined regions, there will be two multipactor electric field thresholds: a *lower multipactor electric field threshold*, responsible for the ignition of the multipactor regime in the region, and an *upper multipactor electric field threshold* beyond which the multipactor extinguishes in the analyzed region. Details on the determination of these multipactor electric field thresholds are given in Section III-C.

For the analyzed geometries, it was found that the *Region A* and *Region C* of the bridge are prone to multipactor for the *non-conditioned* TEEY case, whereas, only the *Region C* is prone to multipactor when using the *fully conditioned* TEEY case. For the impedance transformer, *Section 2* and *Transition 2* are the problematic regions when using the *non-conditioned* TEEY, and only the *Transition 2* remains problematic when it comes to the *fully conditioned* TEEY. We have found that for 3D complex geometries, the conditioning effect on the multipactor electric field thresholds is the same as the one observed in [19]. A reduction in the multipactor electric field range is observed when the surface is conditioned: *i)* the *lower multipactor electric field threshold* is higher for the *fully conditioned* case than that for the *non-conditioned* case. *ii)* The *higher multipactor electric field threshold* is lower for the *fully conditioned* case, than that for the *non-conditioned* case.

B. Determination of the Antenna Electric Fields

The circuit model of one ICRH antenna during its RF conditioning is represented in Fig. 6. In this circuit model, all the components (RF feed-through, T-junction, and impedance transformer) of the *left* and *right* sides of the antenna are taken into consideration using their full-wave models, except for the capacitors that are modelled using an equivalent lumped circuit [23]. To mimic the operational situation, the in-series resistor is set to zero (infinity) when a generator is on (off), while the shunt one is set to infinity (zero). This is done to model accurately the forward impedance seen from the RF window's side when the generator is off.

At a particular frequency of interest, and for each side: *i)* the generator state is chosen – on or off, and the forward power(s) of the on-mode generator(s) is (are) set. *ii)* The capacitors' state is chosen – *tuned* or *detuned* along with the capacitance values for the tuned side(s). Then, solving the self-consistent simulation leads to the determination of the *excited electric fields* in each multipactor region of the bridge and impedance transformer components. The *excited electric fields* are then evaluated in two susceptible zones: the susceptible zone corresponding to the *lower multipactor electric field threshold*, and the one corresponding to the *higher multipactor electric field threshold*, as described in the next section.

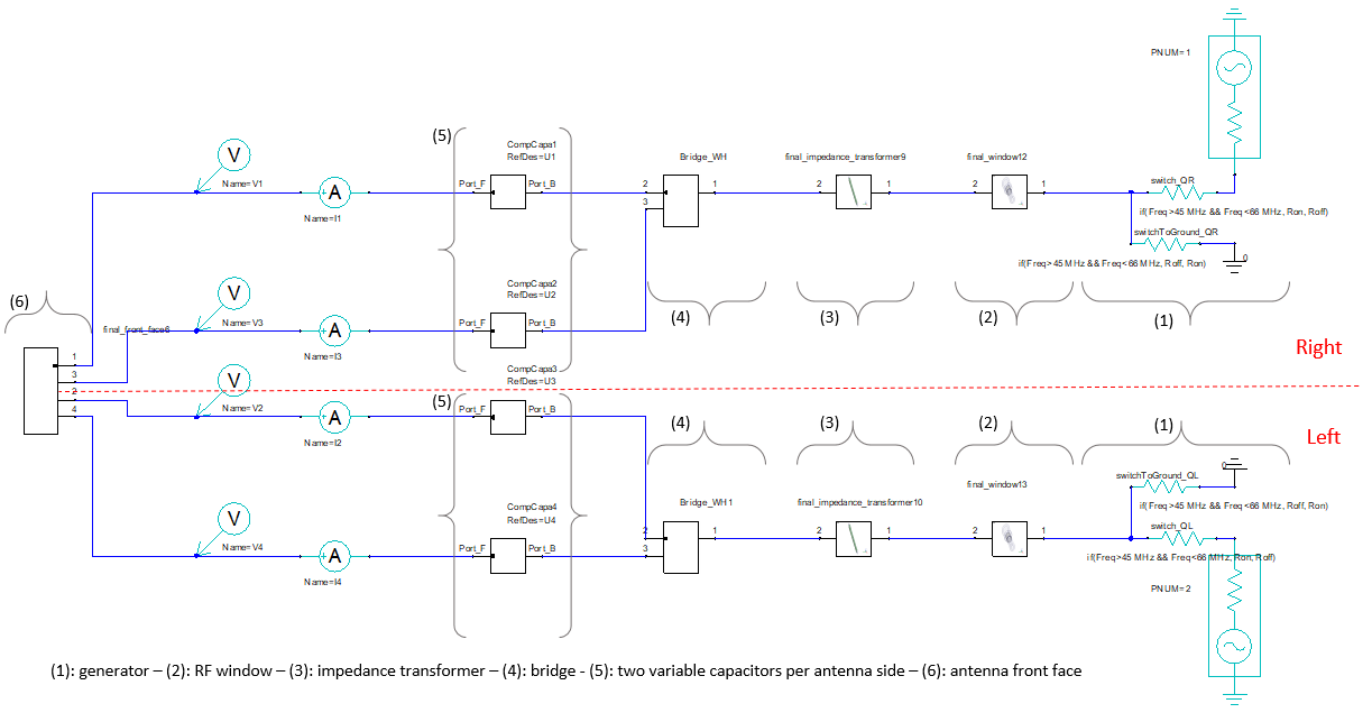

Fig. 6. Circuit model of one ICRH antenna, during its RF conditioning phase, where both sides of the antenna are modelled to take into account the RF coupling. Each side of the antenna is composed of: (1) – one generator that could be in one of two possible states (on or off), (2) – one RF ceramic feed-through window, (3) – one impedance transformer, (4) – one bridge, (5) – two variable capacitors. Both sides of the ICRH antenna are connected through: (6) – one front face. The operator of the antenna could only configure the RF frequency, powers and phases of the generators and the values of the capacitors.

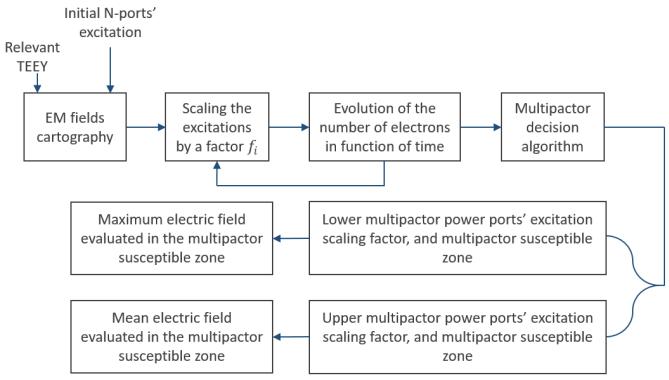

Fig. 7. The steps summarizing the applied methodology for the determination of the multipactor electric fields thresholds for each of the components' regions.

C. Multipactor Analysis Under Standing Wave

We are interested in determining the lower and upper multipactor electric field thresholds regardless of the reflection coefficient – as the ICRH antennas are prone to regimes under mixed or standing wave patterns resulting from the combination of incident and reflected waves.

In the first step (Fig. 7), the electromagnetic (EM) fields cartography is generated for a given region after choosing the power ports' excitation and the appropriate TEEY curve, before being imported to the multipactor tool analysis (Spark-3D). In the second step, the multipactor analysis is done by an iterative scaling of the ports' excitation by a factor f_i, before making a decision on the existence of multipactor based on the number of electrons' evolution in time [19]. The output of this step is the determination of the lower and upper scaling multipactor factors, as well as the multipactor susceptible zones. The multipactor susceptible zone corresponds to the region's part where the multipactor conditions are simultaneously fulfilled. In the last step, we have extracted two multipactor criteria: *i)* the relevant physical quantity for the lower multipactor threshold, is the peak value of the electric field's magnitude evaluated in the multipactor susceptible zone. We refer to this physical quantity as the *lower multipactor electric field threshold*. *ii)* The relevant physical quantity for the upper multipactor threshold is the mean (average) value of the electric field's magnitude evaluated in the multipactor susceptible zone. We refer to this physical quantity as the *upper multipactor electric field threshold*. It was found that the developed criteria are constant regardless of any variability in the initial ports' excitation, *i.e.* reflection coefficient. The intention behind the idea is that under SW patterns if the multipactor conditions are met, the multipactor ignition is near the SW electric field's peaks, whereas its extinction is near the SW electric field's nodes [20].

IV. Results

In this section, multipactor regions are given by the lower and upper generators' forward powers triggering multipactor on each antenna side as a function of the antenna frequency range. Red curves represent the results of the *non-conditioned* TEEY, for the *left* and the *right* sides of the antenna. Black

curves represent the results of the *fully conditioned* TEEY. The nominal generator forward power range during RF conditioning is represented as a grey band.

A. Case 1

In this first case, both generators are powered with the same forward power and both capacitors' sides are *tuned*. Because of the antenna symmetry and vacuum loading (non-anisotropic), it is expected to obtain similar multipactor power thresholds on both sides. The thresholds illustrated in Fig. 8 confirms this expectation as, for both TEEY cases, *left* generator's forward powers triggering multipactor on its side are the same as for the *right* side.

Surface conditioning reduces the multipactor thresholds, as also shown in [19]. In particular, it tends to increase the lower generators' forward power thresholds and decrease the upper generators' ones, thus reducing the multipactor domain.

The regions where multipactor takes place are deduced by looking at the generators' forward powers responsible for triggering multipactor in each component. The bridge's and impedance transformer's different multipactor regions, corresponding to the *right* and *left* sides of the antenna, are represented in Fig. 9, and Fig. 10 respectively. The solid lines correspond to the results for the *non-conditioned* case (red curve of Fig. 2), while the dashed lines correspond to the *fully-conditioned* case (black curve of Fig. 2). Results of the *left* side of the antenna are identical to those of the *right* side. It also shows that the surface conditioning suppresses multipactor in the *Region A* of the bridge, the *Section 2* of the impedance transformer. In addition, the multipactor zone is reduced within the *Region C* of the bridge, and the *Transition 2* of the impedance transformer.

B. Case 2

In the second case, only the generator of the *right* side is energized. Hence, multipactor-triggering powers correspond to the *right* side generator's forward powers. In other terms, we are interested in determining the forward powers for the *right* generator triggering multipactor in both the powered side (*right*) and in the non-powered side (*left*), the latter being caused by the cross-talk between antenna sides.

Fig. 11, represents the minimal and maximal forward powers, triggering multipactor in the *left*, and the *right* sides of the RF-conditioned antenna, for the *non-conditioned* TEEY in red, and the *fully conditioned* TEEY in black. This figure reveals that, in the RF-conditioning nominal power range, and within the ICRH frequency range, leaving the off-mode side's capacitors *tuned* leads to the trigger of multipactor in both sides of the antenna, for the *non-conditioned* TEEY measurements. Nevertheless, the probability of multipactor trigger on the non-powered side is reduced when the surface of the antenna is fully conditioned. Therefore, the very remarkable similarity between **Case 1** and **Case 2**, especially for the *non-conditioned* TEEY curve, is explained by the state of the capacitors. In particular, for the TEEY measurements before any conditioning, the multipactor-triggering generator's powers for the bridge of the *right* (on) and *left* (off) sides

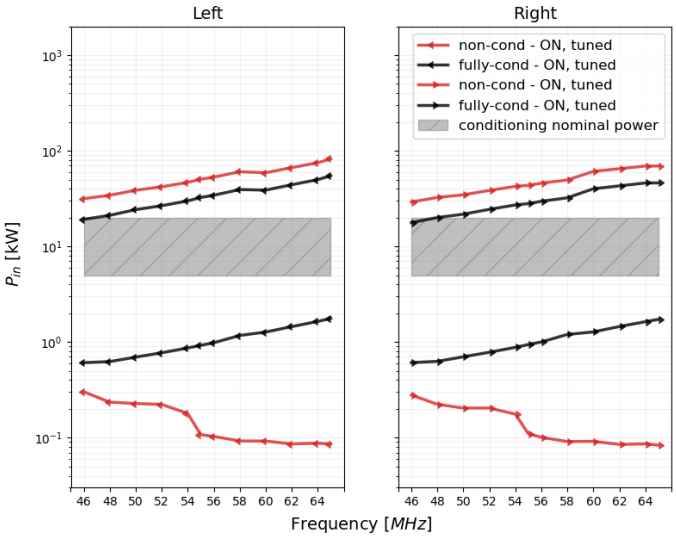

Fig. 8. The generators' forward powers, as a function of the ICRH frequency range, responsible for triggering the multipactor in its corresponding antenna side (the figure of left (right) corresponds to the results of the *left* (*right*) side of the antenna). The red (respectively black) curves correspond to the minimal and maximal forward powers triggering multipactor in one antenna side for the *non-conditioned* (*fully conditioned*) TEEY cases represented in red (black) in Fig. 2. The dashed grey band corresponds to the nominal RF conditioning operational powers.

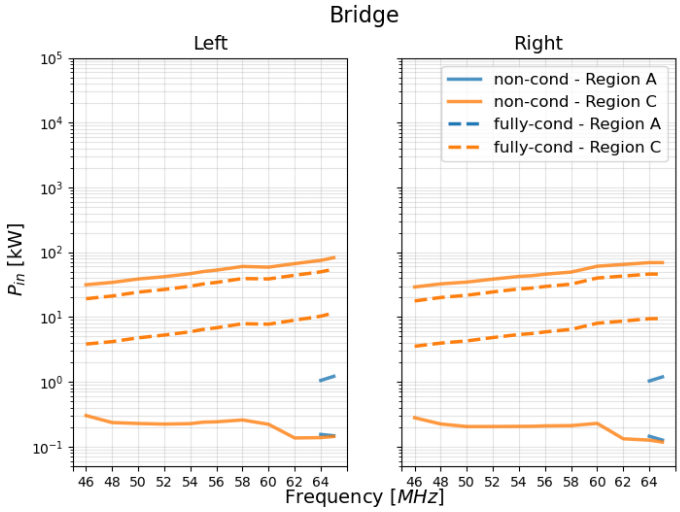

Fig. 9. Left (Right) – In solid lines, the generators' forward powers, as a function of the ICRH frequency range, responsible for triggering multipactor in the multipactor-prone regions (*Region A* and *Region C*) of the bridge for the *left* (*right*) side of the antenna. The solid lines are the results for the *non-conditioned* TEEY case. In dashed lines, the generator's forward powers, as a function of the ICRH frequency range, responsible for triggering multipactor in the multipactor-prone region (*Region C*) of the bridge for the *left* (*right*) side of the antenna. The dashed lines are the results for the *fully conditioned* TEEY case. *Region A* is not prone to multipactor for the *fully conditioned* TEEY case.

of the antenna (represented in Fig. 12), are very comparable even though one of the sides is not even powered. When the capacitors of the off-mode side are *tuned*, the power is coupled to the off-mode side and is responsible for triggering the multipactor in the bridge, the nearest component to the front face, due to the sides' cross-talk. Nevertheless, this is not the case for the impedance transformer, as shown in Fig. 13.

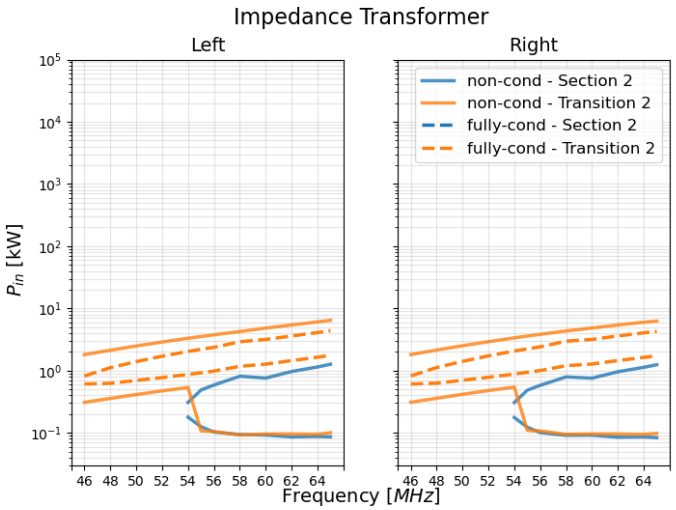

Fig. 10. Left (Right) – In solid lines, the generators' forward powers, as a function of the ICRH frequency range, responsible for triggering multipactor in the multipactor-prone regions (*Section 2* and *Transition 2*) of the impedance transformer for the *left* (*right*) side of the antenna. The solid lines are the results for the *non-conditioned* TEEY data curve. In dashed lines, the generator's forward powers, as a function of the ICRH frequency range, responsible for triggering multipactor in the multipactor-prone region (*Transition 2*) of the impedance transformer for the *left* (*right*) side of the antenna. The dashed lines are the results for the *fully conditioned* TEEY data curve. *Section 2* is not prone to multipactor for the *fully conditioned* TEEY case.

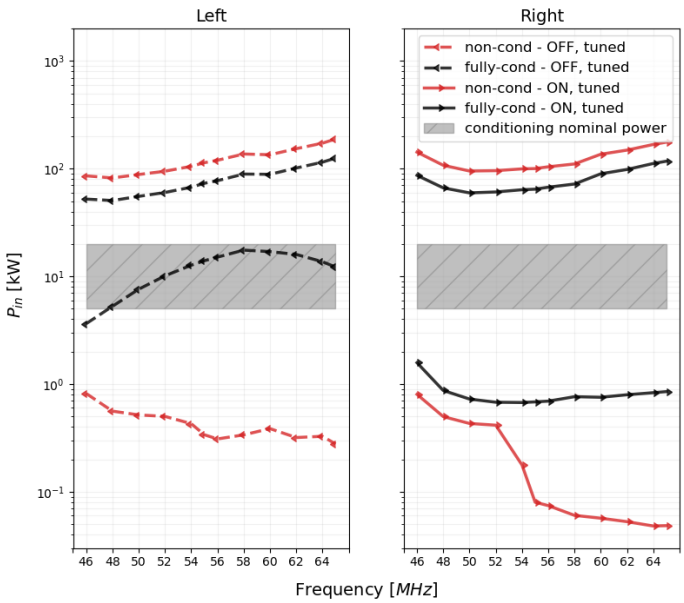

Fig. 11. The *right*-side generator's forward powers, as a function of the ICRH frequency range, responsible for triggering the multipactor in the different antenna sides (the figure of left (right) corresponds to the results of the *left* (*right*) side of the antenna). The red (respectively black) curves correspond to the minimal and maximal forward powers of the on-mode generator, triggering multipactor in one antenna side for the *non-conditioned* (*fully conditioned*) TEEY data curve represented in red (black) in Fig. 2. The dashed grey band corresponds to the nominal RF conditioning operational powers.

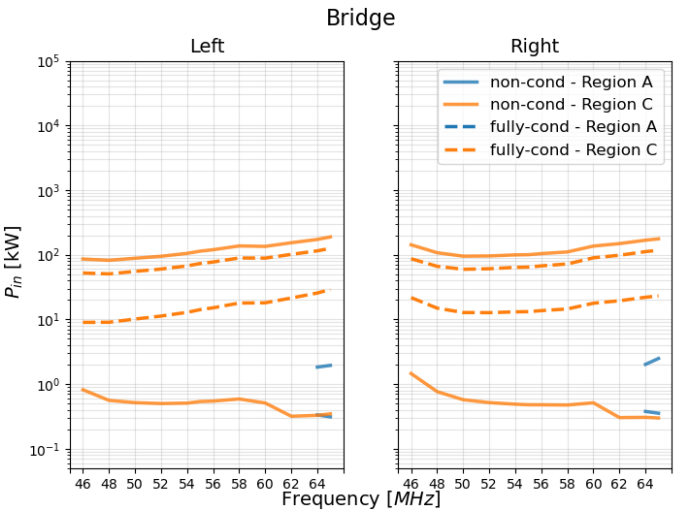

Fig. 12. Left (Right) – In solid lines, the on-mode generator's forward powers, as a function of the ICRH frequency range, responsible for triggering the multipactor in the multipactor-prone regions (*Region A* and *Region C*) of the bridge for the *left* (*right*) side of the antenna. The solid lines are the results for the *non-conditioned* TEEY data curve. In dashed lines, the on-mode generator's forward powers, as a function of the ICRH frequency range, responsible for triggering multipactor in the multipactor-prone region (*Region C*) of the bridge for the *left* (*right*) side of the antenna. The dashed lines are the results for the *fully conditioned* TEEY data curve. *Region A* is not prone to multipactor for the *fully conditioned* TEEY case.

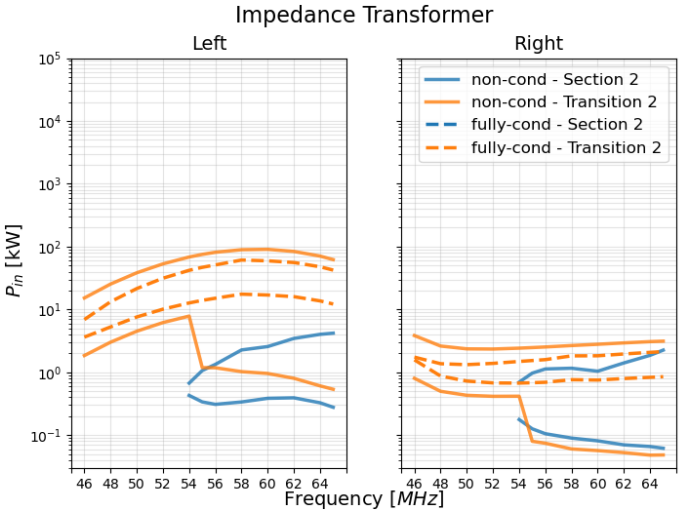

Fig. 13. Left (Right) – In solid lines, the on-mode generator's forward powers, as a function of the ICRH frequency range, responsible for triggering the multipactor in the multipactor-prone regions (*Section 2* and *Transition 2*) of the impedance transformer for the *left* (*right*) side of the antenna. The solid lines are the results for the *non-conditioned* TEEY data curve. In dashed lines, the on-mode generator's forward powers, as a function of the ICRH frequency range, responsible for triggering multipactor in the multipactor-prone region (*Transition 2*) of the impedance transformer for the *left* (*right*) side of the antenna. The dashed lines are the results for the *fully conditioned* TEEY data curve. *Section 2* is not prone to multipactor for the *fully conditioned* TEEY case.

At a given frequency, the forward power needed to trigger multipactor inside the impedance transformer of the off-mode side (*left*) is higher than for the on-mode side (*right*) as the impedance transformer is farther from the capacitors than the bridge.

C. Case 3

In this last case, the capacitors of the off-mode (*left*) side are *detuned* while the capacitors of the on-mode (*right*) side

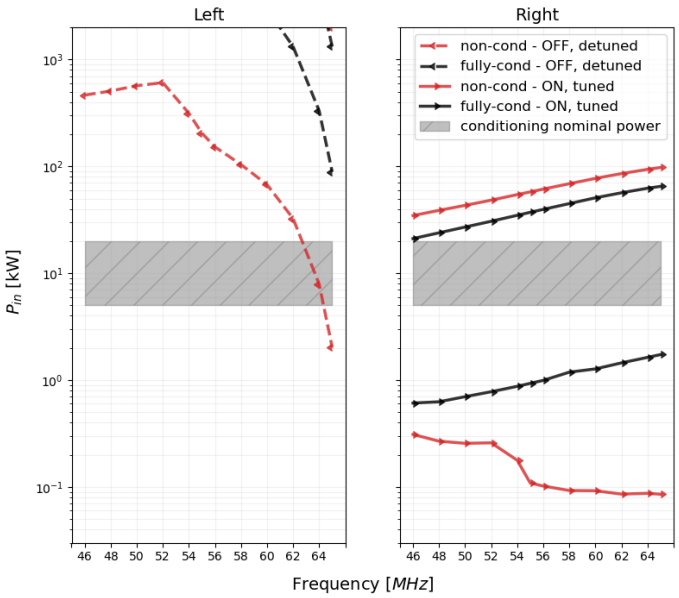

Fig. 14. CASE DESCRIPTION. Same caption as Fig. 11.

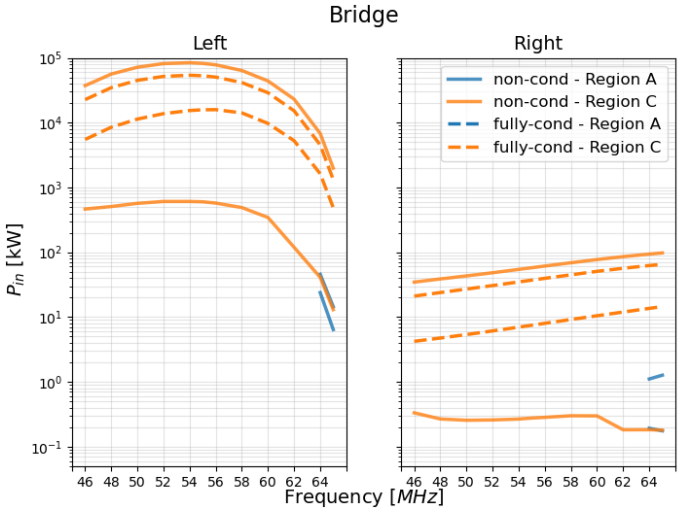

Fig. 15. CASE DESCRIPTION. Same caption as Fig. 12.

are *tuned*. On-mode generator's forward powers responsible for multipactor trigger are illustrated in Fig. 14. This figure shows that, for the *non-conditioned* case, in the nominal power range for RF-conditioning, and within the frequency range $[46-63]$ MHz, multipactor can be triggered only in the on-mode side and not the off-mode side. Nevertheless, within $[63-65]$ MHz, multipactor can still be triggered inside the components of both sides of the antenna. Moreover, for the *fully conditioned* case, within the ICRH frequency range, multipactor is only triggered on the on-mode side, while the off-mode side is not prone to multipactor.

The differences between Fig. 14 and Fig. 11 are attributed to the capacitors' states of the off-mode side, which are respectively *detuned*, and *tuned*. This result reveals the necessity of having *detuned* capacitors to avoid or reduce multipactor on the non-powered side. This conclusion is particularly relevant to operation, as, during RF conditioning on a single side, safety

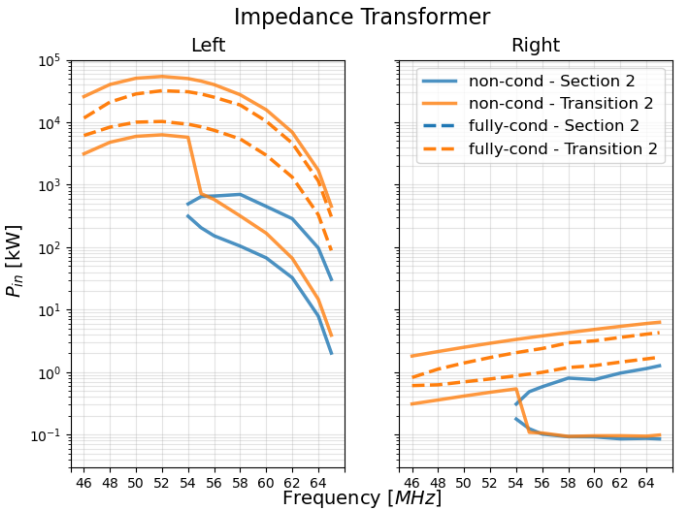

Fig. 16. CASE DESCRIPTION. Same caption as Fig. 13.

interlocks do not depend on the off-mode side.

For **Case 3**, the forward powers needed to trigger multipactor inside the bridge and the impedance transformer (shown in Fig. 15, and Fig. 16) of the non-powered side are higher than those seen in **Case 2**, as the cross-talk to the off-mode side is reduced when the capacitors are *detuned*.

V. Conclusion

In this paper, we proposed a self-consistent methodology to determine the WEST ICRH antenna forward powers triggering multipactor during RF conditioning under vacuum. This general methodology led to the determination of the multipactor locations and power thresholds for relevant operational scenarios.

The results obtained indicate the best strategy to follow for the RF operators to minimize risks associated with multipactor during this phase, which is to detune the capacitors of the off-mode side of the ICRH antenna when only one side is active. In addition, the methodology was applied for two extreme cases of the silver-coated antenna's surface properties, that is for *non-conditioned* and *fully conditioned* surfaces. It is shown that the reduction of the TEEY associated with the surface conditioning reduces the multipactor power domain or even totally suppresses it.

Further studies will concentrate on modelling the multipactor triggering powers during plasma operation in WEST, taking into account the cross-coupling between different antennas through the plasma. This methodology will also be extended to include the front face, capacitors and geometries having multiple TEEY, *i.e.*, the ceramic vacuum feed-through. The methodology exposed in this work is generic and can be used to study the occurrence of multipactor on larger antennas, for example in ITER.

Acknowledgments

This work has been carried out within the framework of the EUROfusion Consortium, funded by the European Union via the Euratom Research and Training Programme (Grant

Agreement No 101052200 — EUROfusion). Views and opinions expressed are however those of the author(s) only and do not necessarily reflect those of the European Union or the European Commission. Neither the European Union nor the European Commission can be held responsible for them.

REFERENCES

[1] W. Helou, L. Colas, J. Hillairet, D. Milanesio, P. Mollard, A. Argouarch, G. Berger-By, J.-M. Bernard, Z. Chen, J.-M. Delaplanche, P. Dumortier, F. Durodié, A. Ekedahl, N. Fedorczak, F. Ferlay, M. Goniche, J. Jacquot, E. Joffrin, X. Litaudon, G. Lombard, R. Maggiora, R. Magne, J.-C. Patterlini, M. Prou, R. Volpe, K. Vulliez, and K. Winkler, "Radio-frequency electrical design of the west long pulse and load-resilient icrh launchers," *Fusion Engineering and Design*, vol. 96-97, pp. 473–476, 2015. Proceedings of the 28th Symposium On Fusion Technology (SOFT-28).

[2] J. Hillairet, P. Mollard, L. Colas, W. Helou, G. Urbanczyk, J.-M. Bernard, J.-M. Delaplanche, F. Durand, N. Faure, P. Garibaldi, G. Lombard, C. Bourdelle, C. Desgranges, E. Delmas, R. Dumont, A. Ekedahl, F. Ferlay, M. Goniche, C. Guillemaut, G. T. Hoang, P. Maget, R. Volpe, Y. Song, Q. Yang, Z. Chen, Y. Wang, H. Xu, S. Yuan, Y. Zhao, F. Durodie, E. Lerche, R. Ragona, N. Bertelli, M. Ono, S. Shiraiwa, V. Bobkov, C. Klepper, C. Lau, E. Martin, B. Lu, R. Maggiora, D. Milanesio, K. Vulliez, G. Wallace, and W. Team, "WEST actively cooled load resilient ion cyclotron resonance heating system results," *Nuclear Fusion*, vol. 61, p. 096030, Aug. 2021. Publisher: IOP Publishing.

[3] J. Vaughan, "Multipactor," *IEEE Transactions on Electron Devices*, vol. 35, pp. 1172–1180, July 1988.

[4] R. Udiljak, D. Anderson, M. Lisak, V. E. Semenov, and J. Puech, "Multipactor in a coaxial transmission line. I. Analytical study," *Physics of Plasmas*, vol. 14, p. 033508, March 2007.

[5] P. T. Fransworth, "Television by electron image scanning," *Journal of the Franklin Institute*, vol. 218, pp. 411 – 444, October 1934.

[6] V. Petit, M. Taborelli, H. Neupert, P. Chiggiato, and M. Belhaj, "Role of the different chemical components in the conditioning process of air exposed copper surfaces," *Physical Review Accelerators and Beams*, vol. 22, p. 083101, August 2019.

[7] V. D. Shemelin and S. A. Belomestnykh, *Multipactor in Accelerating Cavities*. Switzerland: Springer, 2020.

[8] T. P. Graves, S. J. Wukitch, B. LaBombard, and I. H. Hutchinson, "Effect of multipactor discharge on Alcator C-Mod ion cyclotron range of frequency heating," *Journal of Vacuum Science & Technology A: Vacuum, Surfaces, and Films*, vol. 24, pp. 512–516, May 2006.

[9] M. Goniche, C. El Mhari, M. Francisquez, S. Anza, J. Belo, P. Hertout, and J. Hillairet, "Modelling of power limit in RF antenna waveguides operated in the lower hybrid range of frequency," *Nuclear Fusion*, vol. 54, p. 013003, January 2014.

[10] K. H. Jang, S. J. Wang, H. H. Wi, K. Saito, J. H. Kim, H. Y. Lee, and J. G. Kwak, "Design of multipactor-suppressed high-power VFT for helicon current drive in KSTAR," *Fusion Engineering and Design*, vol. 161, p. 111960, Dec. 2020.

[11] R. Woode and J. Petit, "Diagnostic investigations into the multipactor effect, susceptibility zone measurementes and parameters affecting a discharge," technical report 1556, ESA-ESTEC, 1989.

[12] H. Kim, J. Verboncoeur, and Y. Lau, "Modeling rf window breakdown: from vacuum multipactor to rf plasma," *IEEE Transactions on Dielectrics and Electrical Insulation*, vol. 14, 08 2007.

[13] E. Sorolla, *Contribution to Modeling Multipactor and Corona Discharges in High Power Electromagnetic Fields*. PhD thesis, EPFL, 2012.

[14] F. Höhn, W. Jacob, R. Beckmann, and R. Wilhelm, "The transition of a multipactor to a low-pressure gas discharge," *Physics of Plasmas*, vol. 4, pp. 940–944, April 1997.

[15] E. W. B. Gill and A. Von Engel, "Starting potentials of high-frequency gas discharges at low pressure," *Proceedings of the Royal Society of London, Series A. Mathematical and Physical Sciences*, vol. 192, pp. 446–463, February 1948.

[16] J. Vaughan, "A new formula for secondary emission yield," *IEEE Transactions on Electron Devices*, vol. 36, no. 9, pp. 1963–1967, 1989.

[17] M. A. Furman and M. T. F. Pivi, "Probabilistic model for the simulation of secondary electron emission," *Phys. Rev. ST Accel. Beams*, vol. 5, p. 124404, Dec 2002.

[18] N. Fil, M. Belhaj, J. Hillairet, and J. Puech, "Multipactor threshold sensitivity to total electron emission yield in small gap waveguide structure and TEEY models accuracy," *Physics of Plasmas*, vol. 23, p. 123118, December 2016.

[19] E. Al Hajj Sleiman, J. Hillairet, M. Belhaj, and S. Dadouch, "Evaluation of multipactor thresholds for coaxial lines subject to surface conditioning for the west ion cyclotron antenna," *Fusion Engineering and Design*, vol. 185, p. 113325, 2022.

[20] A. M. Perez, C. Tienda, C. Vicente, S. Anza, J. Gil, B. Gimeno, V. E. Boria, and D. Raboso, "Prediction of multipactor breakdown thresholds in coaxial transmission lines for traveling, standing, and mixed waves," *IEEE Transactions on Plasma Science*, vol. 37, October 2009.

[21] G. Romanov, "Stochastic features of multipactor in coaxial waveguides for travelling and standing waves," Tech. Rep. ERMILAB-PUB-11-003-TD, Fermi National Accelerator Lab.(FNAL), Batavia, IL (United States), 2011.

[22] E. Somersalo, P. Yla-Oijala, and D. Proch, "Analysis of multipacting in coaxial lines," in *Proceedings Particle Accelerator Conference*, vol. 3, pp. 1500–1502, May 1995.

[23] J. Hillairet, "RF network analysis of the WEST ICRH antenna with the open-source python scikit-RF package," *AIP Conference Proceedings*, vol. 2254, p. 070010, Sept. 2020. Publisher: American Institute of Physics.